Molecular Modeling Connect
ISSN: 3105-3734
2026, Article ID. 2026.0015, Cite as: https://doi.org/10.69709/MolModC.2026.195329

SCIFINITI PUBLISHING

Research Article

OPEN ACCESS

Computational Exploration of Mutant SARS-CoV-2 Main Protease as a Target for Binding and Inhibition Attributes Utilizing Antiviral Drugs for Therapeutic Application

Sudheer Kumar Katari[✉,1,*,†] **Chandu Sai Kanakala**[✉,1] **Anil Kumar Singh**[✉,2,*,†]

[1] Department of Biotechnology, Vignan's Foundation for Science, Technology and Research, Vadlamudi-522213, Guntur, India
[2] Academy of Scientific and Innovative Research (AcSIR), Ghaziabad-201002, India
[†] Equally contributed to this work.

Article History
Received: November 02, 2025 Accepted: April 20, 2026 Published: June 22, 2026

Abstract
Mutations in Mpro of SARS-CoV-2 have resulted in resistance to previously known inhibitors and other drugs. Inhibiting Mpro is a viable option for the development of effective therapeutic drugs that target SARS-CoV-2 and related viruses. The current work assessed 10 antiviral drugs—Acyclovir, Remdesivir, Sofosbuvir, Atazanavir, Cidofovir, Indinavir, Lopinavir, Oseltamivir, Galidesivir, and Favipiravir—based on the capacity to bind and inhibit mutant Mpro by employing multiple computational methods. The computational physical-chemical characteristics and SSEs revealed comparable results across WT and mutant versions of Mpro. The Mpro-Indinavir docked complex was recognized as the top-ranked molecule, exhibiting a binding affinity of -8.07 ± 0.06 Kcal/mol and a *K*i value of 1.21 μM. In this, hydrogen bond interactions were found between THR-26 and GLN-189 residues. The binding affinity among selected compounds was found to be in a range of -5.37 ± 0.40 to -8.07 ± 0.06 Kcal/mol. The top four ranked docked complexes were evaluated for stability, structural conformational, and other key parameters by implementing Desmond MD simulation of 100 ns, which subsequently confirmed the stability and system equilibrium state till the end of the simulation period. The results indicate that several antiviral drugs have adequate binding potential and inhibitory efficiency, as anticipated by *K*i. This suggests that compounds with notable binding and other properties can be effectively repurposed as promising therapeutic candidates for mutant Mpro inhibition. Nevertheless, theoretical results necessitate the subsequent experimental validation to presume the practical efficacy of the screened drugs.

Keywords:
docking; main protease; binding affinity; inhibition constant; MD simulation

1. Introduction

In late 2019, a highly transmissible and pathogenic coronavirus, known as SARS-CoV-2, emerged, leading to a global pandemic of acute respiratory disease, which was recognized as COVID-19. This infection triggers a threat to public safety and human health [1]. The COVID-19 pandemic accounted for over 18 million deaths and substantially destabilized the world economy, with continued repercussions [2]. As a consequence of the rapid evolutionary nature, the global viral population has noticed a significant increase in the frequency of dozens of mutations, including those that enhance its transmissibility and enable it to escape human immune responses [3]. The estimated mutation rate for SARS-CoV-2 is around 1×10^{-6}–

* **Corresponding Authors:**
Sudheer Kumar Katari, Department of Biotechnology, Vignan's Foundation for Science, Technology and Research, Vadlamudi, Guntur 522213, India, katari319@gmail.com;
Anil Kumar Singh, Academy of Scientific and Innovative Research (AcSIR), Ghaziabad 201002, India, phd.anil@yahoo.com

2×10^{6} mutations per nucleotide per replication cycle, which is in line with earlier estimates for other betacoronaviruses [4]. Antigenic drift, on the other hand, causes Omicron subvariants to change continuously, which is challenging because it makes vaccines less effective and could alter susceptibility to antiviral drugs [5]. According to reports, four antivirals—Ensitrelvir, Nirmatrelvir, Remdesivir, and Molnupiravir—have been approved for the treatment of SARS-CoV-2 infections [5–9]. Among these, Ensitrelvir and nirmatrelvir inhibit the viral 3C-like (3CL) protease (Mpro), a conserved enzyme necessary for polyprotein cleavage and viral replication. On the other hand, remdesivir and molnupiravir block the RdRp, which stops viral genome replication [5]. Resistance to mutations, particularly in Mpro, has emerged as these antivirals are utilized more frequently in clinical contexts, raising concerns about their long-term efficacy [5]. Although Mpro is a highly conserved protease found in many CoVs, no human proteases have comparable cleavage specificity. Therefore, Mpro is an appealing prime target for antiviral drug research for COVID-19 treatment [10]. Moreover, a key benefit of focusing on Mpro is its conserved nature across CoVs. Despite genetic variation present within the CoV family, Mpro exhibits significant sequence and structural similarities among strains. Nirmatrelvir, an approved treatment option for COVID-19, binds covalently to the active site cysteine of the SARS-CoV-2 Mpro. This action effectively blocks enzyme activity and halts viral replication, an approved treatment option for COVID-19, binds covalently to the active site cysteine of the SARS-CoV-2 Mpro [11]. It inhibits viral polyprotein processing, which eventually leads to the cessation of viral replication, by binding covalently and reversibly to the cysteine that is located in the active site of Mpro of SARS-CoV-2 [11]. It has been shown that the influence of nirmatrelvir pressure may cause proximal and active-site mutation in the Mpro of SARS-CoV-2. These mutations reduce the efficacy of the drug and contribute to Paxlovid resistance [11]. As a consequence of this, six mutations in Mpro evolved, each of which included T304I either by alone or in combination with T21I, L50F, T135I, S144A, or A173V. Among these, the A173V + T304I and T21I + S144A + T304I mutations exhibited resistance to Nirmatrelvir that was >20-fold [12]. Alongside the aforementioned antiviral drugs, Remdesivir, Hydroxychloroquine, Favipiravir, Lopinavir, and Ritonavir are commonly used in the treatment of COVID-19 [9,13–15]. Furthermore, reports on HIV protease inhibitors reported that those could be effective in the treatment of COVID-19 as novel strategies [16–19]. The effectiveness of these drugs in combating COVID-19 can vary with their capacity to effectively bind to the SARS-CoV-2 protease, a substantial molecule produced by the coronavirus as it replicates in the human body. To facilitate the advancement of future antiviral drugs for SARS-CoV-2, it is vital to determine the binding affinities of novel compounds, including antivirals, against the mutant form of SARS-CoV-2 Mpro. The present study evaluated the structural and functional attributes of the SARS-CoV-2 Mpro mutant variant using multivalent computational techniques. A selection of ten established antiviral drugs was screened against the mutant Mpro to determine their binding affinity and inhibition potential, with the goal of gaining deeper insights into the inhibitory effects of such. The computational findings revealed that SARS-CoV-2 Mpro protein exhibited significant binding affinities and inhibitory characteristics associated with certain antiviral drugs. However, the experimental or *in vitro* validation is still necessary to support the computational results in the search for novel strategies for dealing with the newly emerged variants of SARS-CoV in the future.

2. Methods

2.1. Selection and Optimization of Antiviral Drugs

A set of ten well-known antiviral drugs was selected (Table 1), based on recently published literature [20–27]. Structural files in 2D coordinates of selected antiviral drugs were retrieved from the PubChem database (https://pubchem.ncbi.nlm.nih.gov) [28]. All retrieved antiviral drugs (ligands) were optimized for energy minimization using the MMFF94 force field in the Avogadro tool (Version 1.2.0) [29,30]. Further, the pH for human physiological conditions (pH 7.4 ± 0.5) was set during ligand preparation for molecular docking by correcting ionization state, tautomers, and stereoisomers, to ensure accurate binding affinity and ligand conformation in the target protein.

2.2. Protein Crystal Structure of SARS-CoV-2 Mpro Preparation and Refinement

Recent findings indicate that mutations in Mpro result in resistance to nirmatrelvir, a recognized inhibitor. For this investigation, the protein crystal structure of SARS-CoV-2 Mpro with a mutation was employed. This was retrieved using PDB ID: 9AUK from the Protein Data Bank (https://www.rcsb.org) [12,31]. The sequence length was 306 residues distributed over two chains (A and B). This deposited model was solved by X-ray diffraction; Resolution: 1.88 Å; R-Value Free: 0.253; R-Value Work: 0.207, and R-Value Observed: 0.210 [12]. This had a mutation

2026, Vol. 3, Article ID. 2026.0015
https://doi.org/10.69709/MolModC.2026.195329

as (A173V). The retrieved structure underwent a rigorous refinement process in which water molecules, co-crystals, and ligands were eliminated. It was then meticulously prepared for the docking simulation by the addition of polar hydrogen, side chain correction, and performing an energy minimization step.

Table 1: Molecular and chemical attributes of selected antiviral drugs for screening of binding and inhibition action on mutant main protease (Mpro).

S.NO	Antiviral Drugs	Molecular Depiction in 2D	Molecular Weight (g/mol)	Molecular Formula
1	Acyclovir	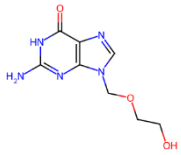	225.20	$C_8H_{11}N_5O_3$
2	Remdesivir	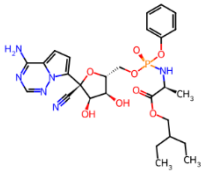	602.6	$C_{27}H_{35}N_6O_8P$
3	Sofosbuvir	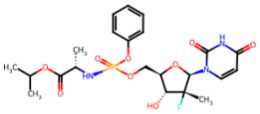	529.5	$C_{22}H_{29}FN_3O_9P$
4	Atazanavir	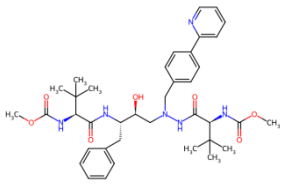	704.9	$C_{38}H_{52}N_6O_7$
5	Cidofovir	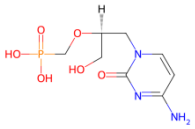	279.19	$C_8H_{14}N_3O_6P$
6	Indinavir	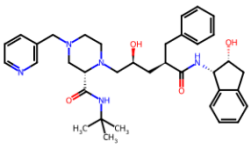	613.8	$C_{36}H_{47}N_5O_4$
7	Lopinavir	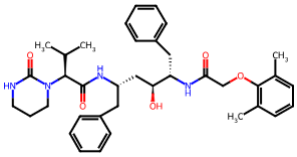	628.8	$C_{37}H_{48}N_4O_5$
8	Oseltamivir		312.40	$C_{16}H_{28}N_2O_4$

Table 1: *Cont.*

S.NO	Antiviral Drugs	Molecular Depiction in 2D	Molecular Weight (g/mol)	Molecular Formula
9	Galidesivir	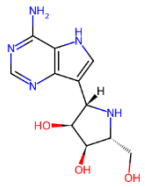	265.27	$C_{11}H_{15}N_5O_3$
10	Favipiravir	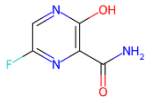	157.10	$C_5H_4FN_3O_2$

2.3. Structural and Physico-Chemical Property Assessment of the Mpro

Structural investigations of two forms of SARS-CoV-2 Mpro, non-mutant (WT) and mutant, were carried out by utilizing their constituent amino acid residues in the protein coordinate file. PDBs as 6Y2E and 9AUK were used for structural overlay using the Needleman-Wunsch algorithm, BLOSUM62 matrix with a cutoff distance of 2 Å. SSEs were also predicted to determine the difference in SSE components (Helix, Sheet, and Coil) using an online web server (https://npsa.lyon.inserm.fr/cgi-bin/npsa_automat.pl?page=/NPSA/npsa_sopma.html). The molecular weight, predicted pI, amino acid/atomic makeup, extinction coefficient, instability index, aliphatic index, and GRAVY are some of the most important key physical and chemical factors of a protein sequence that were also predicted by using the Expasy-ProtParam web tool (https://web.expasy.org/protparam/). The Predicted results for both were compared for each parameter.

2.4. Molecular Docking to Explore Binding Affinity and Molecular Interactions Assessment

The refined protein structure of SARS-CoV-2 mutant Mpro (PDB ID: 9AUK) was utilized in docking analyses with selected optimized ligands. Docking was conducted in GUI mode using the PyRx program (v. 0.8), which integrated AutoDock Vina. A grid box with dimensions of 71 × 74 × 54 Å (X, Y, Z coordinates) was used to allocate the 3D search space on the refined Mpro protein, where the ligands should bind. The binding free energy was considered to be the same with 0 RMSD values when comparing each ligand to the reference compound. After docking, each bound complex was rigorously investigated for possible hydrogen bond interactions and critical amino acid residues occupying the active site, using UCSF Chimera X and the Discovery Studio visualizer (v 16.1.0.15350) software [32,33].

2.5. Inhibition Constant (*Ki*) Calculation

After docking, the inhibition constant (*K*i) was calculated from the final Gibbs free energy of binding (ΔG) by implementing the following formula: $Ki = \exp(\Delta G/RT)$, where R is the universal gas constant (1.985×10^{-3} kcal mol^{-1} K^{-1}), and T is the temperature (298.15 K). *K*i was employed to predict the effectiveness of inhibitors (Docked ligands).

2.6. Validation of Docked Complexes to Get Insight into Stability and Structural Changes by Desmond MD Simulation

Docking is not effective enough for assuming various parameters of structural and functional conformational changes. MD simulation was conducted using Desmond (v2024.4) to explore changes in the conformation of the protein–ligand complex within the solvent system [34]. The OPLS forcefield was employed within an orthorhombic cubic box, centering the complex while filling the space with TIP3P water molecules and buffers, maintaining a distance of 10 Å [34]. The system was neutralized by adding ions, such as Na^+ and Cl^-, to the boundary condition box volume in a random manner [34]. The MD simulation was conducted under the isothermal isobaric ensemble (NPT) with a temperature of 310 K, pressure of 1 atm, and thermostat relaxation time of 200 ps. The Nosé-Hoover thermostat and the Martyne–Tobias—-Klein barostat approaches were employed to maintain the pressure and temperature scale at 310 K and 1 atm, respectively, during MD simulations [35]. The 100 ns NPT phase serves as a crucial period for data collection, enabling the observation of stable molecular behavior, protein conformational changes, and ligand-binding interactions on a 100 ns scale. Post simulation parameters were evaluated for depth analyses and the findings were concluded.

2026, Vol. 3, Article ID. 2026.0015
https://doi.org/10.69709/MolModC.2026.195329

3. Results

3.1. Structural and Physico-Chemical Property Assessment of the MPro

Three-dimensional structures contain essential information for visualizing structural attributes, regardless of the presence of a bound ligand. The 3D structures of SARS-CoV-2 Mpro non-mutant (WT) and mutant were predicted, and compared by superimposing both using the protein coordinates file (PDB ID: 6Y2E and 9AUK). The structures were further compared with structural alignment, which has been represented in cartoon style (Figure 1). The SSE values of the three components were determined to be comparable: 24.18% (Helix), 28.76% (Sheet), and 47.06% (Coil). Furthermore, the physico-chemical properties predicted by ProtParam were evaluated for both variants. The remarkably similar molecular weight was underscored by the similarity of the constituent amino acid residues (306 for both variants), as 33796.64 (Da) for the non-mutant (WT) and 33824.69 (Da) for the mutant. Negatively charged residues (Asp + Glu) in both variants were found to be 26, while positively charged residues (Arg + Lys) were counted as 22. No significant differences were found in other parameters, as listed in Table 2.

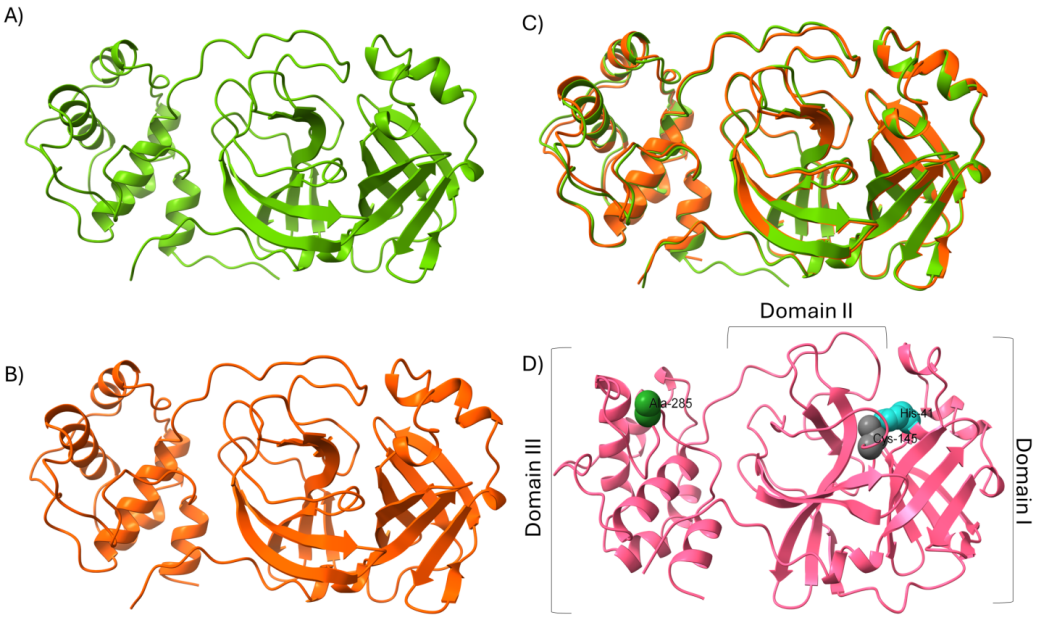

Figure 1: Structural analyses of SARS-CoV-2 Mpro. (**A**) Depiction of a cartoon render of Mpro (WT), image generated from PDB 6Y2E, in a single unit by removing the existing ligand. (**B**) Depiction of a cartoon render of Mpro (Mutant), image generated from PDB 9AUK, in a single unit by removing the existing ligand. (**C**) Depiction of a structure overlay to compare similarity by alignment of residues with residues with an RMSD cutoff value of 2 Å. (**D**) Depiction of a cartoon with marked vital residues present in domains.

Table 2: Predicted physicochemical and secondary structural analyses of non-mutant and mutant main protease.

	Parameter	Main Protease (6Y2E)	Main Protease Mutant (9AUK)
Physical and chemical	Residues count	306	306
	Theoretical pI	5.95	5.95
	Molecular weight in Da	33796.64	33824.69
	Molecular formula	$C_{1499}H_{2318}N_{402}O_{445}S_{22}$	$C_{1501}H_{2322}N_{402}O_{445}S_{22}$
	Negatively charged residues (Asp + Glu)	26	26
	Positively charged residues (Arg + Lys)	22	22
	Instability index	27.65	27.37
	Aliphatic index	82.12	82.75
	Grand average of hydropathicity (GRAVY)	−0.019	−0.011

Table 2: *Cont.*

Parameter		Main Protease (6Y2E)	Main Protease Mutant (9AUK)
Secondary structure elements	Helix	24.18%	24.18%
	sheet	28.76%	28.76%
	Coil	47.06%	47.06%

3.2. Molecular Docking to Explore Binding Affinity, and Molecular Interactions Assessment: Post-Docking Analyses

The binding affinities and potential molecular interactions between mutant Mpro-antiviral drugs were investigated using docking. The docked complexes were analyzed individually for binding affinity and active site residues implicated in H-bond interactions, and the results were reported in mean ± SD, n = 3. The Mpro-Indinavir complex exhibited the lowest binding affinity at −8.07 ± 0.06 Kcal/mol in comparison to the reference (Nirmatrelvir). Key interacting residues consisted of THR-26 and GLN-189, which are involved in an H-bond interaction. The Mpro-Sofosbuvir complex exhibited a binding affinity of −7.50 ± 0.26 Kcal/mol, indicating a relative second rank among all docked complexes. H-bond interactions occurred among HIS-41, GLY-143, SER-144, CYS-145, and HIS-163 residues. Detailed docking findings have been listed in Table 3. The docking assessment demonstrated that the binding energy of each ligand varied significantly, with values ranging from −5.37 ± 0.40 to −8.07 ± 0.06 Kcal/mol. The lowest ΔG pose of the top four complexes with 2D interactions is portrayed in Figure 2.

Table 3: Docking analyses of docked antiviral drugs to the main protease mutant variant with key binding, interacting amino acid residue, and Inhibition constant (*K*i).

S.No	Complex (MPro + Antiviral Drugs)	Binding Affinity (Kcal/mol) (Mean ± SD, n = 3)	Interacting Amino Acid Residues	Contact Bond Type	Inhibition Constant (*K*i) μM
1	Acyclovir	−5.57 ± 0.06	PHE-140, LEU-141, GLY-143, SER-144, CYS-145, GLU-166	H-bond	82.4
2	Remdesivir	−6.73 ± 0.31	ARG-131, LYS-137, THR-199, ASN-238, ASP-289	H-bond	11.6
3	Sofosbuvir	−7.50 ± 0.26	HIS-41, GLY-143, SER-144, CYS-145, HIS-163	H-bond	3.16
4	Atazanavir	−6.97 ± 0.46	LYS-102, TYR-154, SER-158, ARG-298	H-bond	7.73
5	Cidofovir	−5.87 ± 0.29	ARG-131, THR-199, ASN-238	H-bond	49.7
6	Indinavir	−8.07 ± 0.06	THR-26, GLN-189	H-bond	1.21
7	Lopinavir	−7.30 ± 1.30	CYS-145, MET-165	H-bond	4.41
8	Oseltamivir	−6.10 ± 0.17	ASN-142, GLY-143, GLU-166	H-bond	33.6
9	Galidesivir	−6.40 ± 0.46	PHE-140, ASN-142, SER-144, CYS-145, HIS-163, GLU-166	H-bond	20.2
10	Favipiravir	−5.37± 0.40	GLN-110, THR-111, ASN-151, ASP-295, ARG-298	H-bond	115.00
*	Nirmatrelvir	−7.80± 0.61	HIS-163, GLU-166, THR-190	H-bond	1.91

* was used as a known reference compound.

2026, Vol. 3, Article ID. 2026.0015
https://doi.org/10.69709/MolModC.2026.195329

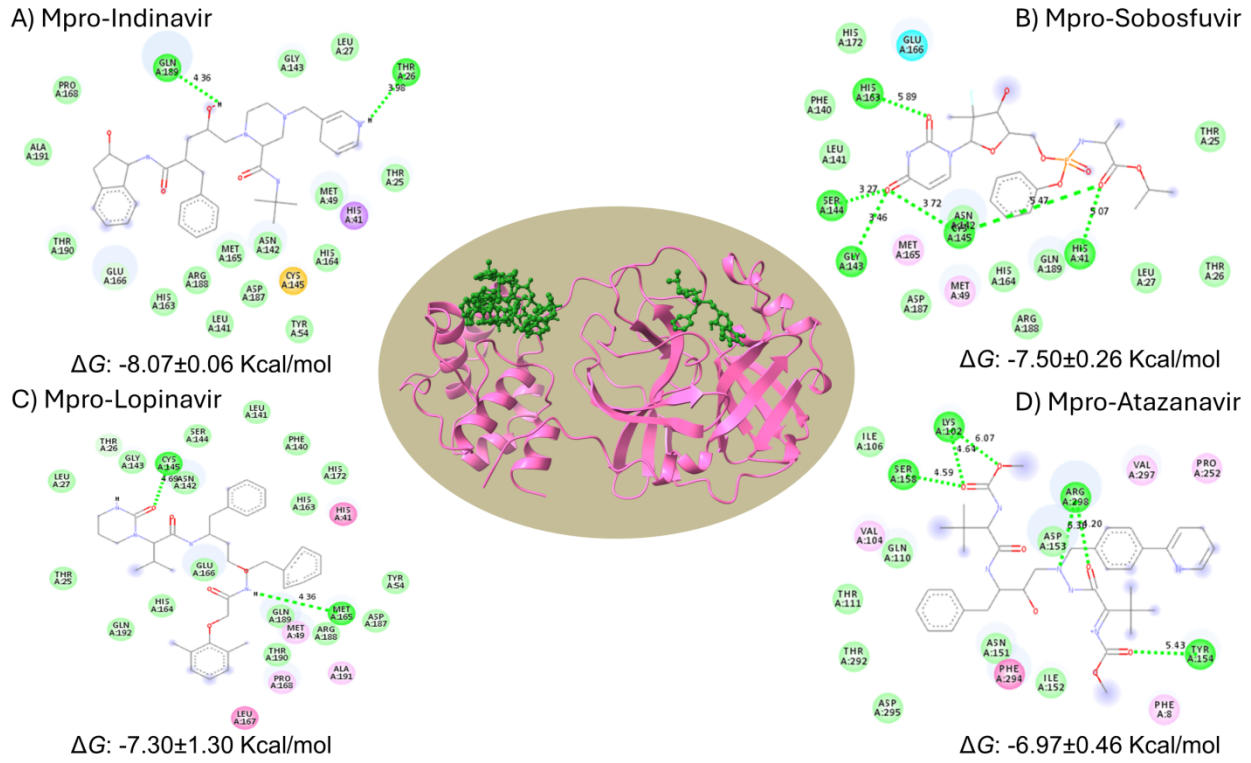

Figure 2: Best-ranked docking pose of ligand-Mpro. The docking pose is marked with an H-bond and bond length. (**A**) 2D interaction of Mpro-Indinavir associated with H-Bond. (**B**) 2D interaction of Mpro-Sofosbuvir associated with H-Bond. (**C**) 2D interaction of Mpro-Lopinavir associated with H-Bond. (**D**) 2D interaction of Mpro-Atazanavir associated with H-Bond.

3.3. Inhibition Constant (*Ki*) Calculation

In the present study, *Ki* was used to determine how well a ligand binds to a target to exert inhibitory action. It was calculated as the concentration required to produce half-maximum inhibition. Calculated *Ki* from estimated free binding energy (ΔG); a lower *Ki* value can define a stronger binding with significant potency. Mpro-Indinavir, the best-ranked docked complex, was determined to have a *Ki* concentration value of 1.21 μM, which was significant to inhibit the Mpro (Mutant). For Favipiravir, the *Ki* value was calculated as 115.00 μM, indicating a far higher concentration value than the best-ranked compound. *Ki* was predicted for each antiviral, and the value was determined to be within the range of 1.21 to 115.00 μM (Table 3).

3.4. Validation of Docked Complexes to Get Insight into Stability and Structural Changes by Desmond MD Simulation

Four top-ranked docked complexes were subjected to a 100 ns MD Simulation to evaluate the stability of the complexes and to analyze the protein fluctuations associated with the docked ligand. A selection of key parameters outlined below was selected to be further elaborated in detail.

3.4.1. Protein-Ligand RMSD Analyses

The protein–ligand complexes were simulated for 100 ns to assess stability and protein fluctuations with bound ligands. The RMSD of Cα atoms was computed to assess the comprehensive structural changes and deviations of the complexes (Protein-Ligand) throughout the simulation. The average RMSD value was observed to be < 2.5 Å for all top four docked complexes. Top-ranked complex Mpro-Indinavir exhibited stability at the end of simulation with an average RMSD of 2.1 Å (Figure 3-A). Second-ranked complex Mpro-Sofosbuvir exhibited stability at the end (beyond 50 ns) of the simulation with an average RMSD of 2.1 Å (Figure 3-B). Mpro-Lopinavir exhibited stability from 0 to 100 ns with an average RMSD of 2.0 Å (Figure 3-C). Last-ranked complex Mpro-Atazanavir exhibited instability with ligand till the end of the simulation run with an average RMSD of 2.2 Å (Figure 3-D).

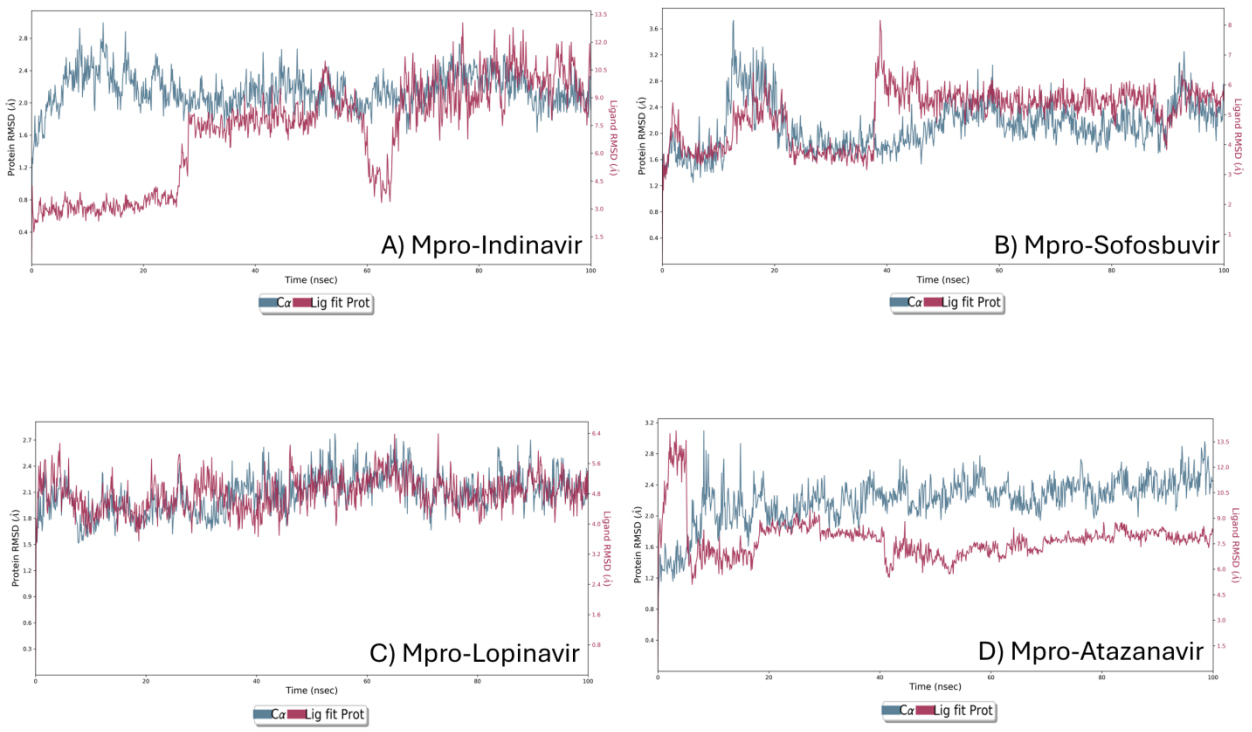

Figure 3: Protein-ligand RMSD plots of the top-ranked four complexes. (**A**) Portray of Mpro-Indinavir complex RMSD over 100 ns. (**B**) Portray of Mpro-Sofosbuvir complex RMSD over 100 ns. (**C**) Portray of Mpro- Lopinavir complex RMSD over 100 ns. (**D**) Portray of Mpro-Atazanavir complex RMSD over 100 ns. All complexes except D can be observed for system stability at the end of the simulation with an average RMSD of less than 2.5 Å.

3.4.2. Protein RMSF Analyses

An RMSF investigation was conducted to evaluate the fluctuations of proteins when bound to ligands. The RMSF values for each protein residue throughout the simulation period provide insightful details about the mobility and flexibility of the residues. According to the predicted RMSF values, the majority of protein residues exhibited little fluctuation throughout the simulation, remained less than 1.5. Å. Mpro-Indinavir complex observed for an average RMSF value of 1.0 Å. The highest fluctuation was observed within GLY-302 (6.8 Å), SER-301 (5.0 Å), and CYS-300 (3.8 Å) residues (Figure 4-A). Mpro- Sofosbuvir complex observed for an average RMSF value of 1.1 Å. Highest fluctuation were observed among SER-1 (5.2 Å), GLY-302 (5.5 Å), SER-301 (3.3 Å) residues (Figure 4-B). Mpro-Lopinavir complex observed for an average RMSF value of 1.1 Å. Highest fluctuation were observed among GLY-302 (4.5 Å), GLY-2 (3.4 Å), SER-301 (2.7 Å) residues (Figure 4-C). Mpro-Atazanavir complex was found to have the highest fluctuation among SER-1 (6.1 Å), GLY-2 (4.7 Å), GLY-302 (4.6 Å) residues with an average RMSF value of 1.1 Å (Figure 4-D).

3.4.3. Protein-Ligand Contacts Analyses

Protein-ligand interactions were analyzed for binding stability, demonstrating the presence of hydrogen bonding. Interaction histograms and 2D maps illustrate the frequency of residues throughout the trajectory. The Mpro-Indinavir complex reveals that the residues THR-199, TYR-237, ASN-238, TYR-239, LEU-271, LEU-272, ASN-274, MET-276, ASN-277, GLY-278, ALA-285, LEU-287, and GLU-288 engage in formation of H-bond contacts (Figure 5-A). The Mpro- Sofosbuvir complex reveals that the residues GLN-19, THR-24, THR-26, ASN-28, HIS-41, SER-46, TYR-118, ASN-119, GLY-120, ASN-142, CYS-145, HIS-164, GLU-166, and GLN-189 engage in formation of H-bond contacts (Figure 5-B). The Mpro-Lopinavir complex revealed that the residues PHE-3, TRP-207, MET-276, ASN-277, GLY-278, ARG-279, LEU-286, LEU-287, and GLU-288 were engaged in H-bond interactions (Figure 5-C). The last fourth-ranked complex, Mpro- Atazanavir complex, revealed that the residues HIS-80, LYS-90, LYS-236, TYR-237, ASN-238, TYR-239, LEU-271, LEU-272, GLN-273, ASN-274, GLY-275, MET-276 were engaged in H-bond interactions (Figure 5-D).

2026, Vol. 3, Article ID. 2026.0015
https://doi.org/10.69709/MolModC.2026.195329

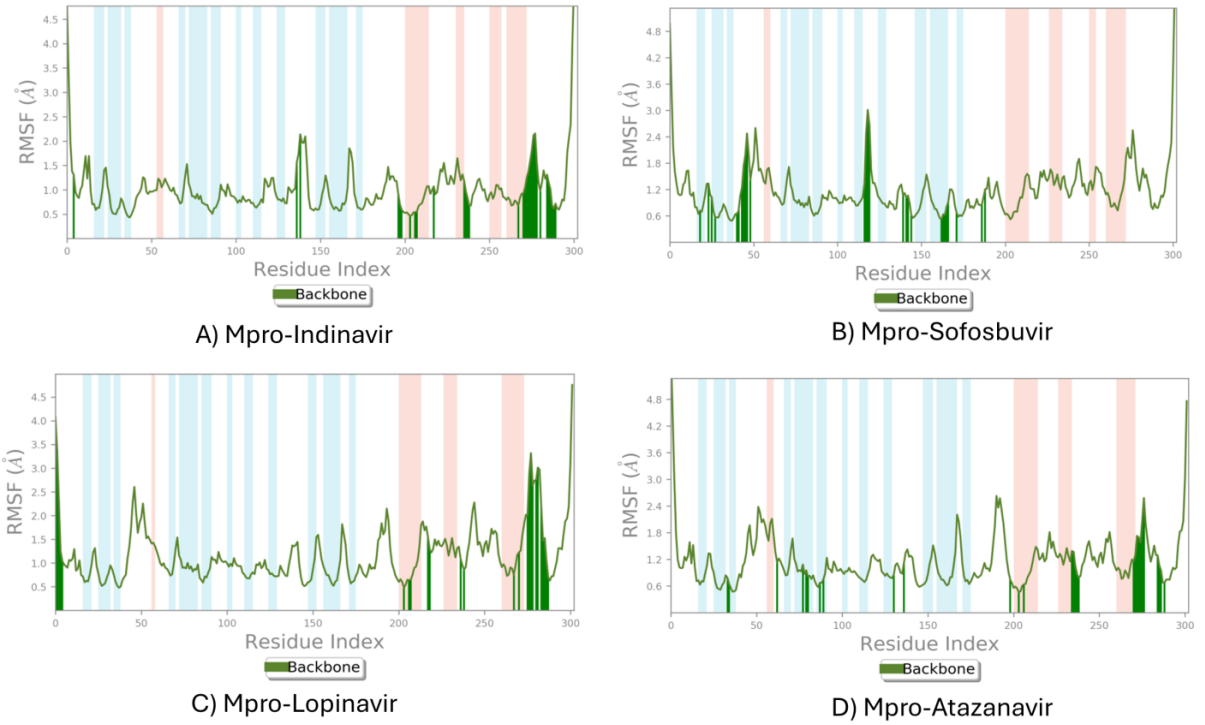

Figure 4: (**A**) Portray of Mpro-Indinavir RMSF plot over 100 ns. (**B**) Portray of Mpro-Sofosbuvir RMSF plot over 100 ns over 100 ns. (**C**) Portray of Mpro-Lopinavir RMSF plot over 100 ns. (**D**) Portray of Mpro-Atazanavir complex RMSF plot over 100 ns.

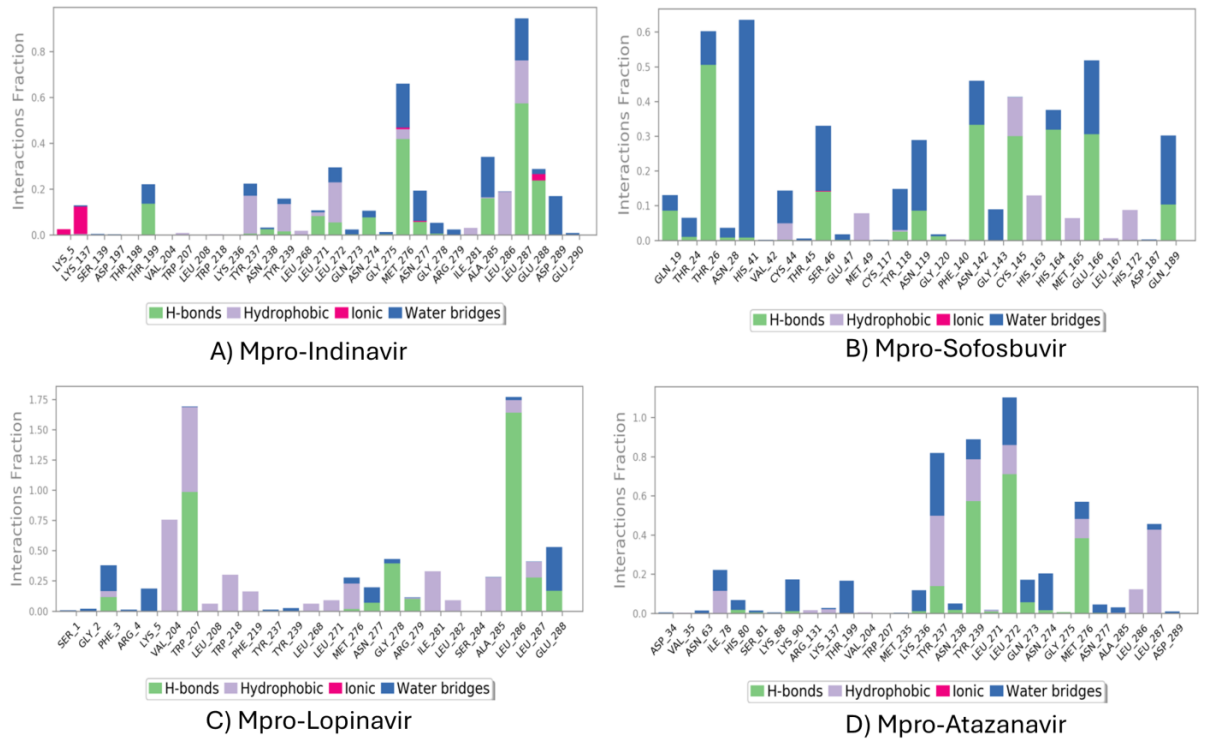

Figure 5: (**A**) Portray of Mpro-Indinavir P-L contacts plot with H-bond interactions among corresponding amino-acid residues. (**B**) Portray of Mpro-Sofosbuvir P-L contacts plot with H-bond interactions among corresponding amino-acid residues. (**C**) P-L contacts plot with H-bond interactions among corresponding amino-acid residues. (**D**) Portray of Mpro-Atazanavir P-L contacts plot with H-bond interactions among corresponding amino-acid residues.

3.4.4. Post-Simulation Energy Assessment

Analyzing potential energy after simulations in Desmond is essential for evaluating system stability, the quality of equilibration, and the structural energy landscapes. This analysis was conducted with the help of Schrödinger's Maestro interface tools following the completion of MD simulations. Post simulation P_E was assessed in a range of −119333.748 to −127536.512 Kcal/mol. The comparative plot of P_E is depicted in Figure 6.

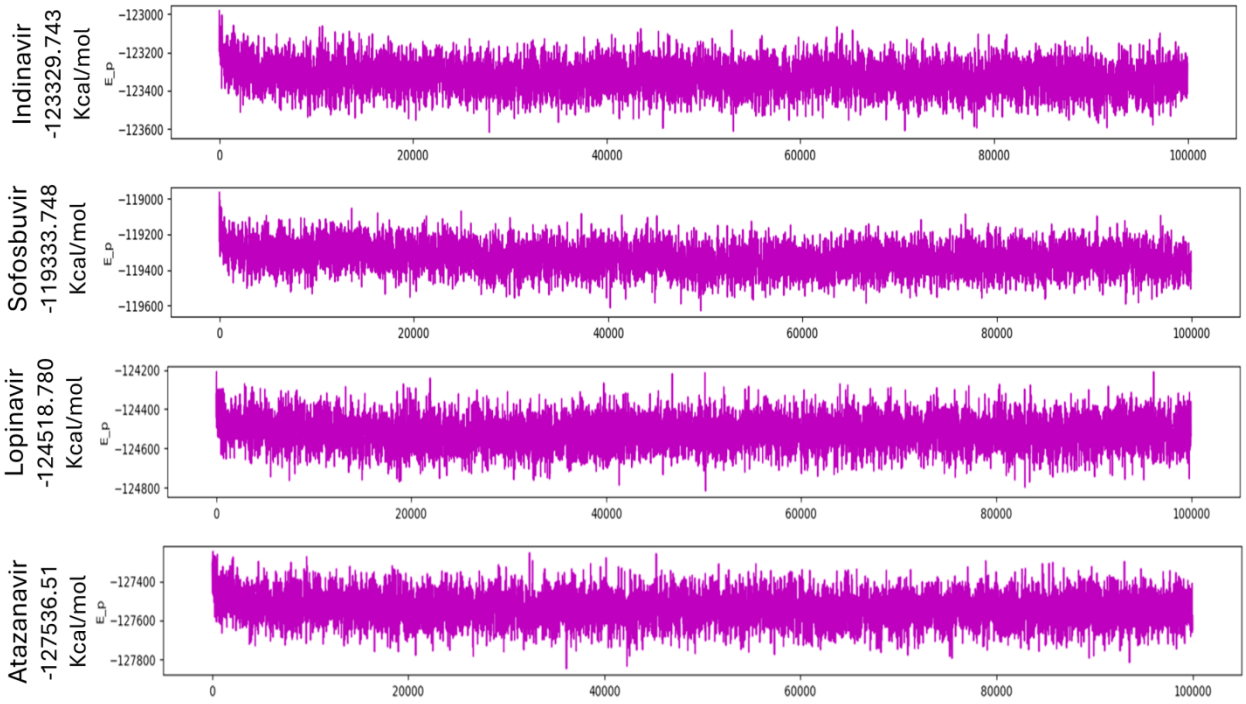

Figure 6: Post-simulation P_E energy plot of the four best-ranked complexes.

4. Discussion

The structural and functional characteristics of a protein play a vital role in defining its biological properties. The protein-ligand complexes that achieve the highest scores indicate the potential for off-target interactions of the ligand. The active site residues of a protein or receptor play a crucial role in the binding of drugs (ligands). In fact, these active site residues serve as the crucial molecular framework for ligand interaction. The Mpro stands out as a vital target for exploring inhibitors intended for combating COVID-19. In recent years, a multitude of studies have documented the existence of potential inhibitors that target Mpro [36–38]. Nirmatrelvir, a recognized oral Mpro inhibitor for severe COVID-19 treatment, encounters efficacy challenges stemming from evolved mutations in Mpro that are linked to resistance against Nirmatrelvir [39]. Considering the likelihood of unexpected toxicity associated with covalent inhibitors due to their high reactivity, it is crucial to focus on the development of noncovalent inhibitors for SARS-CoV-2 Mpro [10,40]. In this challenge, the discovery of a potential molecule may prove advantageous in tackling future medical issues related to COVID-19. Ten antiviral drugs that target the SARS-CoV-2 Mpro mutant variant were investigated in this study in an attempt to determine the binding affinities and inhibitory capabilities as a possible therapeutic option. Computational physical-chemical properties exhibited comparable parameters, which further concluded that non-mutant and mutant variants have similar values in predicted parameters, i.e., Theoretical pI, Instability index, Aliphatic index, and a few others, as listed in Table 2. In addition to this, SSE pointed out that both of the Mpro variants had similar values for helix, sheet, and coil, ranging from 24.18% to 47.06%. This might possibly be due to a similar and the same number of constituent amino acid residues. The antiviral drugs that were chosen revealed a significant binding affinity score in comparison to the reference compound (Nirmatrelvir), which distinguished them from all other ligands (antiviral drugs).

2026, Vol. 3, Article ID. 2026.0015
https://doi.org/10.69709/MolModC.2026.195329

The Mpro-Indinavir complex revealed the lowest binding affinity among all docked complexes, achieving a remarkable score of -8.07 ± 0.06 Kcal/mol. This complex engaged in H-bond interactions with THR-26 and GLN-189 residues. Conversely, a relatively weak binding affinity was noted for the Mpro-Favipiravir complex, which had a binding affinity score of -5.37 ± 0.40 (Kcal/mol), including GLN-110, THR-111, ASN-151, ASP-295, and ARG-298 residues, involved in H-bond interactions. Further *K*i, was calculated to estimate the concentration required by the ligand to inhibit Mpro theoretically. *K*i for the top-ranked complex was estimated as 1.21 μM, while 115.00 μM for Favipiravir. The effective range of *K*i was estimated to be between 1.21 μM and 115.00 μM, with the lowest values being more effective than the highest. Active site residues such as ARG, LYS, PHE, LEU, GLY, SER, CYS, GLU, THR, ASN, ASP, HIS, TYR, GLN, and MET played a crucial role in H-bond formation within the Mpro-antivirals. After docking, the docked complexes were validated by conducting a 100 ns MD simulation to obtain structural conformational information and stability assessment of the bound ligand at the active site of the protein. During this phase, only the top four best-ranked complexes were examined primarily to evaluate P-L RMSD, Protein RMSF, Protein-ligand contacts, and post-simulation analyses. The simulation concluded with archived stability in only three complexes, with an average RMSD of less than 2.2 Å. PHE, GLN, THR, ASN, HIS, SER, LYS, TYR, GLY, CYS, GLU, TRP, LEU, MET, ARG, and ALA were among the common amino acid residues that were observed to be involved in H-bond contacts. Further post-simulation P_E energy was also assessed to conclude the simulation over 100 ns. The results indicated that a limited number of antiviral drugs have the potential to bind to Mpro and theoretically inhibit it at specific concentrations in the form of *K*i. Such information could be employed to repurpose antiviral drugs as potent Mpro inhibitors. Moreover, appropriate experimental investigations may be conducted to corroborate computational results as a feasible therapeutic approach for treating future viruses with characteristics similar to SARS-CoV-2.

5. Conclusions

The architecture of proteins functions as a binding framework for target ligands or therapeutic drugs, facilitating the alteration of the natural activities of those. Thus, the architecture of proteins provides a conceptual basis for comprehending ligand binding to ascertain inhibitory potential. The presented study carried out a theoretical exploration with structural analyses, uncovering potent binding affinity attributes for the inhibitory effects of selected antiviral drugs on mutant Mpro. The binding affinity was observed with a range that varied from -5.37 ± 0.40 to -8.07 ± 0.06 Kcal/mol, while the *K*i values were noted to be between 1.21 to 115.00 μM for the selected antiviral drugs. The binding affinity and *K*i accurately confirmed an acceptable binding mechanism and inhibitory concentration of the antiviral drugs in μM concentration. Subsequently, MD simulations revealed stable ligand interactions over a duration of 100 ns. Binding affinity is a valuable method for screening antiviral drugs on mutant Mpro, but further *in vitro* or cell line experimental validation is required to further analyze these candidates for drug-like activity practically. The computational findings discussed in this study could pave the way for repurposing antiviral drugs, transforming them into effective therapeutics against mutant Mpro of SARS-CoV-2 and similar emerging viruses in the future.

List of Abbreviations

Cα	Carbon Alpha
CoV	Coronaviruses
COVID-19	Coronavirus Disease 2019
Da	Dalton
*K*i	Inhibitory Constant
Mpro	Main Protease
RdRp	RNA-dependent RNA polymerase
RMSD	Root Mean Square Deviation
RMSF	Root Mean Square Fluctuation
SARS-CoV-2	Severe Acute Respiratory Syndrome Coronavirus 2
SSE	Secondary Structure Elements
WT	Wild Type

Author Contributions

S.K.K.: Conceptualization, Data curation, Formal analysis, Investigation, Methodology, Validation, Software, Writingoriginal draft, Writing review & editing, and Supervision. C.S.K.: Data curation, Formal analysis, Investigation, Methodology, Validation, Software, Writing review & editing. A.K.S.: Conceptualization, Data curation, Formal analysis, Investigation, Methodology, Validation, Software, Project administration, Writingoriginal draft, Writing review & editing, Visualization, and Supervision. All authors have read and approved the published version of the manuscript.

Availability of Data and Materials

All data used in the present study were generated from computational experiments and are provided herein. Data

associated with the results are available upon request from the corresponding authors.

Consent for Publication

No consent for publication is required, as the manuscript does not involve any copyright materials or other materials that would necessitate consent. All authors have read and approved the published version of the manuscript.

Funding

The study did not receive any external funding and was conducted using only institutional resources.

Acknowledgments

SKK is highly thankful to VFSTR (Deemed to be University) for providing the faculty seed grant (F.No. VFSTR/REG/A6/30/2023-24/01 dated 16-05-2023). AKS thankfully acknowledges the "Academy of Scientific and Innovative Research (AcSIR)", Ghaziabad, India (An *Institute of National Importance)*

AI Declaration

The authors confirm that no AI tools were used to generate any content of this manuscript.

References

[1] Hu, B.; Guo, H.; Zhou, P.; Shi, Z.L. Characteristics of SARS-CoV-2 and COVID-19. *Nat. Rev. Microbiol.* **2021**, *19*, 141–154. [CrossRef] [PubMed]

[2] Zagórska, A.; Czopek, A.; Fryc, M.; Jończyk, J. Inhibitors of SARS-CoV-2 Main Protease (Mpro) as Anti-Coronavirus Agents. *Biomolecules* **2024**, *14*, 797. [CrossRef] [PubMed]

[3] Haddox, H.K.; Angehrn, G.; Sesta, L.; Jennings-Shaffer, C.; Temple, S.D.; Galloway, J.G.; Hinrichs, A.S.; DeWitt, W.S.; Bloom, J.D.; Iv, F.A.M.; et al. The Mutation Rate of SARS-CoV-2 Is Highly Variable between Sites and Is Influenced by Sequence Context, Genomic Region, and RNA Structure. *Nucleic Acids Res.* **2025**, *53*, gkaf503. [CrossRef] [PubMed]

[4] Markov, P.V.; Ghafari, M.; Beer, M.; Lythgoe, K.; Simmonds, P.; Stilianakis, N.I.; Katzourakis, A. The Evolution of SARS-CoV-2. *Nat. Rev. Microbiol.* **2023**, *21*, 361–379. [CrossRef] [PubMed]

[5] Min, S.C.; Seo, J.-J.; Jeong, J.H.; Kim, B.K.; Park, J.-H.; Lee, J.R.; Lee, D.G.; Lee, G.C.; An, S.H.; Baek, Y.H.; et al. A SARS-CoV-2 Mpro Mutation Conferring Ensitrelvir Resistance Paradoxically Increases Nirmatrelvir Susceptibility. *Nat. Commun.* **2025**, *16*, 10737. [CrossRef] [PubMed]

[6] Mukae, H.; Yotsuyanagi, H.; Ohmagari, N.; Doi, Y.; Yamato, M.; Imamura, T.; Sakaguchi, H.; Sanaki, T.; Sonoyama, T.; Tsuge, Y.; et al. Ensitrelvir as a Novel Treatment Option for Mild-to-Moderate COVID-19: A Narrative Literature Review. *Ther. Adv. Infect. Dis.* **2025**, *12*, 20499361251321724. [CrossRef] [PubMed]

[7] Jayk Bernal, A.; Gomes da Silva, M.M.; Musungaie, D.B.; Kovalchuk, E.; Gonzalez, A.; Delos Reyes, V.; Martín-Quirós, A.; Caraco, Y.; Williams-Diaz, A.; Brown, M.L.; et al. Molnupiravir for Oral Treatment of COVID-19 in Nonhospitalized Patients. *N. Engl. J. Med.* **2022**, *386*, 509–520. [CrossRef] [PubMed]

[8] Hammond, J.; Yunis, C.; Fountaine, R.J.; Luscan, G.; Burr, A.M.; Zhang, W.; Wisemandle, W.; Soares, H.; Baniecki, M.L.; Hendrick, V.M.; et al. Oral Nirmatrelvir–Ritonavir as Postexposure Prophylaxis for Covid-19. *N. Engl. J. Med.* **2024**, *391*, 224–234. [CrossRef] [PubMed]

[9] Beigel, J.H.; Tomashek, K.M.; Dodd, L.E.; Mehta, A.K.; Zingman, B.S.; Kalil, A.C.; Hohmann, E.; Chu, H.Y.; Luetkemeyer, A.; Kline, S.; et al. Remdesivir for the Treatment of COVID-19—Final Report. *N. Engl. J. Med.* **2020**, *383*, 1813–1826. [CrossRef] [PubMed]

[10] Okabe, A.; Carney, D.W.; Tawada, M.; Akther, T.; Aida, J.; Takagi, T.; Dougan, D.R.; Leffler, A.E.; Bell, J.A.; Frye, L.; et al. Discovery of Highly Potent Noncovalent Inhibitors of SARS-CoV-2 Main Protease through Computer-Aided Drug Design. *J. Med. Chem.* **2025**, *68*, 21330–21345. [CrossRef] [PubMed]

[11] Fischer, C.; Lu, J.; van Belkum, M.J.; Demmon, S.; Chen, P.; Wang, C.; Van Oers, T.J.; Lamer, T.; Lemieux, M.J.; Vederas, J.C. Structural Insights into the Nirmatrelvir-Resistant SARS-CoV-2 Mpro L50F/E166A/L167F Triple Mutant-Inhibitor-Complex Reveal Strategies for Next Generation Coronaviral Inhibitor Design. *RSC Med. Chem.* **2025**, *16*, 5032–5040. [CrossRef] [PubMed]

[12] Zhu, Y.; Yurgelonis, I.; Noell, S.; Yang, Q.; Guan, S.; Li, Z.; Hao, L.; Rothan, H.; Rai, D.K.; McMonagle, P.; et al. In Vitro Selection and Analysis of SARS-CoV-2 Nirmatrelvir Resistance Mutations Contributing to Clinical Virus Resistance Surveillance. *Sci. Adv.* **2024**, *10*, eadl4013. [CrossRef] [PubMed]

[13] Cavalcanti, A.B.; Zampieri, F.G.; Rosa, R.G.; Azevedo, L.C.; Veiga, V.C.; Avezum, A.; Damiani, L.P.; Marcadenti, A.; Kawano-Dourado, L.; Lisboa, T.; et al. Hydroxychloroquine with or without Azithromycin in Mild-to-Moderate Covid-19. *N. Engl. J. Med.* **2020**, *383*, 2041–2052. [CrossRef] [PubMed]

[14] Jorge, A. Hydroxychloroquine in the Prevention of COVID-19 Mortality. *Lancet Rheumatol.* **2021**, *3*, e2–e3. [CrossRef] [PubMed]

[15] Dabbous, H.M.; Abd-Elsalam, S.; El-Sayed, M.H.; Sherief, A.F.; Ebeid, F.F.S.; El Ghafar, M.S.A.; Soliman, S.; Elbahnasawy, M.; Badawi, R.; Tageldin, M.A. Efficacy of Favipiravir in COVID-19 Treatment: A Multi-Center Randomized Study. *Arch. Virol.* **2021**, *166*, 949–954. [CrossRef] [PubMed]

[16] Ma, L.; Li, Q.; Xie, Y.; Zhao, J.; Yi, D.; Guo, S.; Guo, F.; Wang, J.; Yang, L.; Cen, S. Repurposing of

HIV/HCV Protease Inhibitors against SARS-CoV-2 3CLpro. *Antivir. Res.* **2022**, *207*, 105419. [CrossRef] [PubMed]

[17] Von Hentig, N. Repositioning HIV Protease Inhibitors and Nucleos(t)ide RNA Polymerase Inhibitors for the Treatment of SARS-CoV-2 Infection and COVID-19. *Eur. J. Clin. Pharmacol.* **2021**, *77*, 1297–1307. [CrossRef] [PubMed]

[18] Yu, W.; Wu, X.; Zhao, Y.; Chen, C.; Yang, Z.; Zhang, X.; Ren, J.; Wang, Y.; Wu, C.; Li, C.; et al. Computational Simulation of HIV Protease Inhibitors to the Main Protease (Mpro) of SARS-CoV-2: Implications for COVID-19 Drugs Design. *Molecules* **2021**, *26*, 7385. [CrossRef] [PubMed]

[19] Majerová, T.; Konvalinka, J. Viral Proteases as Therapeutic Targets. *Mol. Asp. Med.* **2022**, *88*, 101159. [CrossRef] [PubMed]

[20] Mahdi, M.; Mótyán, J.A.; Szojka, Z.I.; Golda, M.; Miczi, M.; Tőzsér, J. Analysis of the Efficacy of HIV Protease Inhibitors against SARS-CoV-2′s Main Protease. *Virol. J.* **2020**, *17*, 190. [CrossRef] [PubMed]

[21] Sultan, A.; Ali, R.; Ishrat, R.; Ali, S. Anti-HIV and Anti-HCV Small Molecule Protease Inhibitors In-Silico Repurposing against SARS-CoV-2 Mpro for the Treatment of COVID-19. *J. Biomol. Struct. Dyn.* **2021**, *40*, 1–15. [CrossRef] [PubMed]

[22] Cao, B.; Wang, Y.; Wen, D.; Liu, W.; Wang, J.; Fan, G.; Ruan, L.; Song, B.; Cai, Y.; Wei, M.; et al. A Trial of Lopinavir–Ritonavir in Adults Hospitalized with Severe COVID-19. *N. Engl. J. Med.* **2020**, *382*, 1787–1799. [CrossRef] [PubMed]

[23] German, E.R.; Jairath, M.K.; Caston, J. Treatment of Long-Haul COVID Patients with Off-Label Acyclovir. *Cureus* **2023**, *15*, e37926. [CrossRef] [PubMed]

[24] Roozbeh, F.; Saeedi, M.; Alizadeh-Navaei, R.; Hedayatizadeh-Omran, A.; Merat, S.; Wentzel, H.; Levi, J.; Hill, A.; Shamshirian, A. Sofosbuvir and Daclatasvir for the Treatment of COVID-19 Outpatients: A Double-Blind, Randomized Controlled Trial. *J. Antimicrob. Chemother.* **2021**, *76*, 753–757. [CrossRef] [PubMed]

[25] Celik, I.; Erol, M.; Duzgun, Z. In Silico Evaluation of Potential Inhibitory Activity of Remdesivir, Favipiravir, Ribavirin and Galidesivir Active Forms on SARS-CoV-2 RNA Polymerase. *Mol. Divers.* **2022**, *26*, 279–292. [CrossRef] [PubMed]

[26] Rahman, M.R.; Banik, A.; Chowdhury, I.M.; Sajib, E.H.; Sarkar, S. Identification of Potential Antivirals against SARS-CoV-2 Using Virtual Screening Method. *Inform. Med. Unlocked* **2021**, *23*, 100531. [CrossRef] [PubMed]

[27] Chaves, O.A.; Sacramento, C.Q.; Ferreira, A.C.; Mattos, M.; Fintelman-Rodrigues, N.; Temerozo, J.R.; Vazquez, L.; Pinto, D.P.; da Silveira, G.P.E.; da Fonseca, L.B.; et al. Atazanavir Is a Competitive Inhibitor of SARS-CoV-2 M(pro), Impairing Variants Replication In Vitro and In Vivo. *Pharmaceuticals* **2022**, *15*, 21. [CrossRef]

[28] Kim, S.; Chen, J.; Cheng, T.; Gindulyte, A.; He, J.; He, S.; Li, Q.; Shoemaker, B.A.; Thiessen, P.A.; Yu, B.; et al. PubChem in 2021: New Data Content and Improved Web Interfaces. *Nucleic Acids Res.* **2021**, *49*, D1388–D1395. [CrossRef] [PubMed]

[29] Halgren, T.A. MMFF94s Option for Energy Minimization Studies. *J. Comput. Chem.* **1999**, *20*, 720–729. [CrossRef]

[30] Hanwell, M.D.; Curtis, D.E.; Lonie, D.C.; Vandermeersch, T.; Zurek, E.; Hutchison, G.R. Avogadro: An Advanced Semantic Chemical Editor, Visualization, and Analysis Platform. *J. Cheminform.* **2012**, *4*, 17. [CrossRef] [PubMed]

[31] Berman, H.M.; Battistuz, T.; Bhat, T.N.; Bluhm, W.F.; Bourne, P.E.; Burkhardt, K.; Feng, Z.; Gilliland, G.L.; Iype, L.; Jain, S.; et al. The Protein Data Bank. *Nucleic Acids Res.* **2000**, *28*, 235–242. [CrossRef] [PubMed]

[32] BIOVIA, Dassault Systèmes. *Discovery Studio, v16.1.0.15350*; Dassault Systèmes: SanDiego, CA, USA, 2021. Available online: https://www.3ds.com/products/biovia/discoverystudio.

[33] Pettersen, E.F.; Goddard, T.D.; Huang, C.C.; Meng, E.C.; Couch, G.S.; Croll, T.I.; Morris, J.H.; Ferrin, T.E. UCSF ChimeraX: Structure Visualization for Researchers, Educators, and Developers. *Protein Sci.* **2021**, *30*, 70–82. [CrossRef] [PubMed]

[34] Gopinath, P.; Kathiravan, M.K. Docking Studies and Molecular Dynamics Simulation of Triazole Benzene Sulfonamide Derivatives with Human Carbonic Anhydrase IX Inhibition Activity. *RSC Adv.* **2021**, *11*, 38079–38093. [CrossRef] [PubMed]

[35] Barrett, T.J.; Minus, M.L. Nosé-Hoover Integrators at-a-Glance: Barostat Integration Has a Demonstrable Effect on Uniaxial Tension Results of Solid Materials. *J. Chem. Theory Comput.* **2025**, *21*, 517–529. [CrossRef] [PubMed]

[36] Tuttle, J.B.; Allais, C.; Allerton, C.M.N.; Anderson, A.S.; Arcari, J.T.; Aschenbrenner, L.M.; Avery, M.; Bellenger, J.; Berritt, S.; Boras, B.; et al. Discovery of Nirmatrelvir (PF-07321332): A Potent, Orally Active Inhibitor of the Severe Acute Respiratory Syndrome Coronavirus 2 (SARS CoV-2) Main Protease. *J. Med. Chem.* **2025**, *68*, 7003–7030. [CrossRef] [PubMed]

[37] Jin, Z.; Du, X.; Xu, Y.; Deng, Y.; Liu, M.; Zhao, Y.; Zhang, B.; Li, X.; Zhang, L.; Peng, C.; et al. Structure of Mpro from SARS-CoV-2 and Discovery of Its Inhibitors. *Nature* **2020**, *582*, 289–293. [CrossRef] [PubMed]

[38] Chan, H.T.H.; Moesser, M.A.; Walters, R.K.; Malla, T.R.; Twidale, R.M.; John, T.; Deeks, H.M.; Johnston-Wood, T.; Mikhailov, V.; Sessions, R.B.; et al. Discovery of SARS-CoV-2 Mpro Peptide Inhibitors from Modelling Substrate and Ligand Binding. *Chem. Sci.* **2021**, *12*, 13686–13703. [CrossRef] [PubMed]

[39] Deschenes, N.M.; Pérez-Vargas, J.; Zhong, Z.; Thomas, M.; Kenward, C.; Mosimann, W.A.; Worrall, L.J.; Waglechner, N.; Li, A.X.; Maguire, F.;

et al. Functional and Structural Characterization of Treatment-Emergent Nirmatrelvir Resistance Mutations at Low Frequencies in the Main Protease (Mpro) Reveals a Unique Evolutionary Route for SARS-CoV-2 to Gain Resistance. *J. Infect. Dis.* **2025**, *232*, e789–e798. [CrossRef] [PubMed]

[40] Zhang, L.; Xie, X.; Luo, H.; Qian, R.; Yang, Y.; Yu, H.; Huang, J.; Shi, P.-Y.; Hu, Q. Resistance Mechanisms of SARS-CoV-2 3CLpro to the Non-Covalent Inhibitor WU-04. *Cell. Discov.* **2024**, *10*, 40. [CrossRef] [PubMed]